Research Article

Mikkel Have Eriksen, Christos Tserkezis, N. Asger Mortensen and Joel D. Cox*

Nonlocal effects in plasmon-emitter interactions

https://doi.org/10.1515/nanoph-2023-0575 Received September 7, 2023; accepted March 19, 2024; published online April 15, 2024

Abstract: Nonlocal and quantum mechanical phenomena in noble metal nanostructures become increasingly crucial when the relevant length scales in hybrid nanostructures reach the few-nanometer regime. In practice, such mesoscopic effects at metal-dielectric interfaces can be described using exemplary surface-response functions (SRFs) embodied by the Feibelman *d*-parameters. Here we show that SRFs dramatically influence quantum electrodynamic phenomena – such as the Purcell enhancement and Lamb shift – for quantum light emitters close to a diverse range of noble metal nanostructures interfacing different homogeneous media. Dielectric environments with higher permittivities are shown to increase the magnitude of SRFs calculated within the specular-reflection model. In parallel, the role of SRFs is enhanced in noble metal nanostructures characterized by large surface-to-volume ratios, such as thin planar metallic films or shells of core-shell nanoparticles, for which the spill-in of electron wave functions enhances plasmon hybridization. By investigating emitter quantum dynamics close to such plasmonic architectures, we show that decreasing the width of the metal region, or increasing the permittivity of the interfacing dielectric, leads to a significant change in the Purcell enhancement, Lamb shift, and visible far-field spontaneous emission spectrum, as an immediate consequence of SRFs. We anticipate that fitting the theoretically modelled spectra to experiments could allow for experimental determination of the d-parameters.

*Corresponding author: Joel D. Cox, POLIMA - Center for Polariton-Driven Light-Matter Interactions, University of Southern Denmark, DK-5230 Odense, Denmark; and Danish Institute for Advanced Study, University of Southern Denmark, DK-5230 Odense, Denmark,

E-mail: cox@mci.sdu.dk. https://orcid.org/0000-0002-5954-6038

Mikkel Have Eriksen and Christos Tserkezis, POLIMA - Center for Polariton-Driven Light-Matter Interactions, University of Southern Denmark, DK-5230 Odense, Denmark, E-mail: meri@mci.sdu.dk (M.H. Eriksen), ct@mci.sdu.dk (C. Tserkezis). https://orcid.org/0000-0002-0159-0896 (M.H. Eriksen). https://orcid.org/0000-0002-2075-9036

N. Asger Mortensen, POLIMA - Center for Polariton-Driven Light-Matter

Interactions, University of Southern Denmark, DK-5230 Odense, Denmark; and Danish Institute for Advanced Study, University of Southern Denmark, DK-5230 Odense, Denmark, E-mail: asger@mailaps.org. https://orcid.org/0000-0001-7936-6264

Keywords: quantum plasmonics; nonlocal response; lightmatter interactions; surface-response functions

1 Introduction

Nanoscale light-matter interactions, and the strong coupling of light with quantum emitters (QEs) such as atoms and molecules, are abundant sources of fundamental physical insights, while offering applications in fields such as optical sensing, photocatalysis, and quantum optics [1]-[3]. In these and other areas, metallic nanostructures that support plasmons - the collective oscillations of conduction electrons - are sought as light-focusing elements that enhance the interaction of QEs with external optical fields [4]-[7]. Meanwhile, in a quantum-electrodynamical context, plasmonic nanostructures are actively explored as subwavelength optical cavities that control the generation of single photons [8]-[11], a key resource for future quantum optical information and communication technologies [12]. Steady progress in the aforementioned frontier research topics has relied crucially on the framework of classical electrodynamics within the local-response approximation (LRA) [13]. However, as the fabrication of plasmonic nanostructures such as metallic nanoparticles (NPs) becomes increasingly advanced, such that the feature size and distance between structures approach the few-nanometer regime, the LRA can no longer accurately estimate the response of the system, as it neglects nonlocal and quantum mechanical corrections in the bulk and at the surface of the metal [13]-[17].

Nonlocal and quantum mechanical phenomena at metal surfaces have been modelled through a series of methods such as descriptions of the bulk response through semi-classical hydrodynamic models [18]-[26] or ab-initio methods such as time-dependent density-functional theory (TDDFT) [27]-[30]. The standard hydrodynamic Drude model (HDM) that relies on the Thomas-Fermi theory with hard-wall boundary conditions describes the motion of the compressible electron gas as a convective fluid and needs amendments to account for surface phenomena such as electron spill-out or spill-in [20], [21], [31], while TDDFT, constituting a more sophisticated method for modelling quantum mechanical phenomena in plasmonic nanostructures, demands huge computational costs and is practically

restricted to few-atom structures. The mesoscopic regime, bridging the micro- and macroscopic realms, necessitates a description that goes beyond the classical LRA and yet is less computationally demanding than ab-initio approaches [32].

Including surface-response functions (SRFs) [33]-[36] in the otherwise classical or semiclassical constitutive relations when solving Maxwell's equations allows us to take into account quantum mechanical phenomena when electrons are confined to small structures in the mesoscopic regime, while still maintaining the simple classical or semiclassical bulk response functions [37]-[41]. Feibelman dparameters are such SRFs that permit the modelling of surface-enabled Landau damping, nonlocality, and electron spill-out or spill-in effects to leading order [42]-[44]. The Feibelman d-parameters, d_{\perp} and d_{\parallel} , are associated with an interface between two materials, depending on the intrinsic properties of these two materials but not on the geometry; dparameters characterizing a specific metal-dielectric interface can be applied in electrodynamic simulations of arbitrary morphologies. The *d*-parameters are often computed using atomistic or ab-initio methods for metal-vacuum interfaces, an approach that is prohibitively time-intensive to tabulate for arbitrary metal-dielectric interfaces. Here, we focus on noble metal interfaces, where d-band screening and spill-in effects cannot be captured by jellium models [29]; we thus resort to finding analytical expressions for the d-parameters using the specular-reflection model (SRM) in combination with HDM for the longitudinal component of the dielectric tensor [45], [46].

When positioned near a plasmonic nanostructure, a quantum emitter (QE), such as a quantum dot or an atom, will exhibit altered emission properties associated with the modified local photonic density of states (LDOS) [47]-[50]. In the specific case of a sodium (Na) NP or interface, the quantum mechanical and nonlocal corrections captured by SRFs result in clear changes to the light emission spectrum of the QE [38], as well as quantum electrodynamical phenomena in the form of the Lamb shift and Purcell enhancement of the QE [40], [42]. Here, we investigate the influence of the *d*-parameters in plasmonic nanostructures comprised of noble metals such as gold (Au) or silver (Ag). Beyond their immediate influence on extinction spectra [51], [52], we show that nonlocal contributions to the emission properties of a nearby QE increase when the permittivity of the interfacing dielectric increases, or the surface area becomes larger compared to the volume of the nanostructure by – for example – increasing the number of interfaces when going from a single extended interface to a thin film, or analogously by substituting a solid spherical NP with a core—shell NP. In particular, the spill-in of electron density at

the surface of noble metals can enhance plasmon hybridization across thin planar films and the shells of core-shell NPs. Our results showcase configurations and situations where the inclusion of quantum mechanical corrections in the mesoscopic regime is of particular importance. These large non-classical corrections might allow for experimental determination of the d-parameters by, e.g., fitting the theory presented here to experimental results [53].

2 Results and discussion

2.1 Surface response functions for arbitrary metal-dielectric interfaces

For a particular dielectric-metal interface spanning the $\mathbf{R} = (x, y)$ plane, the associated Feibelman d-parameters can be obtained regarding the quantum mechanical induced charge and current density in the metal, $\rho(\mathbf{r}) = \rho(z)e^{i\mathbf{Q}\cdot\mathbf{R}}$ and $\mathbf{j}(\mathbf{r}) = \mathbf{j}(z)e^{i\mathbf{Q}\cdot\mathbf{R}}$, respectively, with Q being the in-plane wavevector, from which the parameters are found as [33], [42], [43]:

$$d_{\perp}(\omega) = \frac{\int\limits_{-\infty}^{\infty} \mathrm{d}z z \rho^{\mathrm{ind}}(z, \omega)}{\int\limits_{-\infty}^{\infty} \mathrm{d}z \rho^{\mathrm{ind}}(z, \omega)}, \tag{1a}$$

$$d_{\parallel}(\omega) = \frac{\int\limits_{-\infty}^{\infty} \mathrm{d}z z \partial_{z} j_{\parallel}^{\mathrm{ind}}(z, \omega)}{\int\limits_{-\infty}^{\infty} \mathrm{d}z \partial_{z} j_{\parallel}^{\mathrm{ind}}(z, \omega)}. \tag{1b}$$

$$d_{\parallel}(\omega) = \frac{\int\limits_{-\infty}^{\infty} \mathrm{d}z z \partial_{z} j_{\parallel}^{\mathrm{ind}}(z, \omega)}{\int\limits_{-\infty}^{\infty} \mathrm{d}z \partial_{z} j_{\parallel}^{\mathrm{ind}}(z, \omega)}.$$
 (1b)

In the above expressions, z is taken as the axis normal to the interface, while the system is assumed isotropic in the xy plane. An intuitive physical understanding of the perpendicular parameter, d_{\perp} , is here apparent, corresponding to the centroid of the induced charge density as displayed in the schematic of a metal interfacing a dielectric material in Figure 1(a), where the equilibrium density of electrons in the metal, n, is calculated using a quantum infinite-barrier model and is normalized to the equilibrium density for the infinite electron gas, n_0 [45]. The sign of the real part then differentiates between electron spill-out (Re $\{d_{\perp}\}$ > 0) or the contrary situation of spill-in (Re $\{d_{\perp}\}$ < 0) associated with a high work function. Correspondingly, d_{\parallel} is the centroid of the normal derivative of the in-plane current.

Using these general definitions, one can compute the Feibelman *d*-parameters through *ab-initio* methods, but this requires a new computation for any interface between two different materials. Alternatively, the parameters can be computed using SRM, also known as the semi-classical infinite-barrier (SCIB) model, which

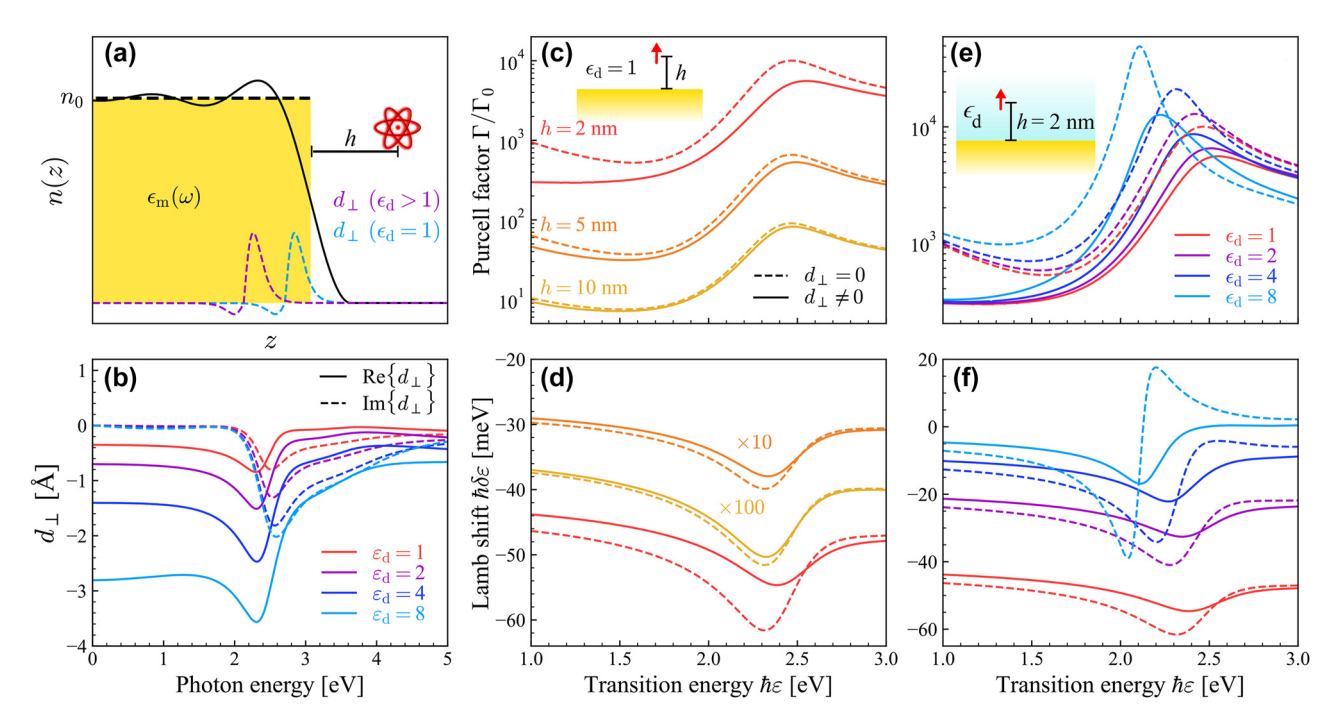


Figure 1: The effect of Feibelman d-parameters from SRM. (a) Schematic of a QE (e.g., an atom) located a distance h from a metal with permittivity $\varepsilon_{\rm m}$ interfacing a dielectric material with permittivity $\varepsilon_{\rm d}$. The electron-density profile n(z) (black solid curve) is calculated using a quantum infinite-barrier model [45], while the induced-charge density (dashed curves, for the two different $\varepsilon_{\rm d}$ indicated in the legend) and the associated perpendicular d_{\perp} -parameters qualitatively show the spill-in depending on $\varepsilon_{\rm d}$. (b) Real (solid curves) and imaginary (dashed curves) parts of the Feibelman d_{\perp} -parameter computed from Eq. (4) for dielectric media with permittivity $\varepsilon_{\rm d}$ (indicated by the color-coded legend) interfacing the metal Au with permittivity $\varepsilon_{\rm m}$ characterized by the model of Ref. [54]. Panels (c–f) show the Purcell factor Γ/Γ_0 and Lamb shift $\delta\varepsilon$ of the emitter as a function of its transition energy $\hbar\varepsilon$ when omitting (dashed curves) and including (solid curves) the Feibelman d-parameters in the metal film response; the effects of separation h (for an emitter in vacuum) and dielectric environment $\varepsilon_{\rm d}$ (for a fixed separation h = 2 nm) are explored in panels (c, d) and (e, f), respectively, for an emitter with transition dipole moment d = 1 e nm.

assumes specular reflection of the conduction electrons at the interface [51], [52]. This results in the parameters [45]:

$$d_{\perp}^{SRM} = -\frac{2}{\pi} \frac{\epsilon_{\rm m} \epsilon_{\rm d}}{\epsilon_{\rm m} - \epsilon_{\rm d}} \int_{0}^{\infty} \frac{\mathrm{d}k_{\rm L}}{k_{\rm L}^2} \left[\frac{1}{\epsilon_{\rm L}(k_{\rm L}, \omega)} - \frac{1}{\epsilon_{\rm m}} \right], \qquad (2a)$$

$$d_{\parallel}^{\text{SRM}} = 0, \tag{2b}$$

where $d_{\parallel}=0$ owing to the fact that the interface is intrinsically charge-neutral in the model, $\epsilon_{\rm m}$ is the classical or semi-classical bulk-metal permittivity, $\epsilon_{\rm d}$ the corresponding permittivity of the dielectric, and $\epsilon_{\rm L}$ is the longitudinal permittivity of the spatially dispersive metal Finally, ω is the angular frequency of the incident light.

To transparently explore nonlocal effects at arbitrary noble metal—dielectric interfaces, rather than following an ab-initio route, we resort to the analytic expressions provided by bulk free electron models. More specifically, we employ the Drude model for $\epsilon_{\rm m}$ in combination with the longitudinal permittivity obtained within HDM,

$$\epsilon_{\rm m}(\omega) = \epsilon_{\rm b}(\omega) - \frac{\omega_{\rm p}^2}{\omega^2 + {\rm i}\omega\gamma},$$
 (3a)

$$\epsilon_{\rm L}(k_{\rm L},\omega) = \epsilon_{\rm b}(\omega) - \frac{\omega_{\rm p}^2}{\omega^2 + {\rm i}\omega\gamma - \beta^2 k_{\rm L}^2}, \tag{3b}$$

where $\beta \propto v_{\rm F}$ contains the dependence on the Fermi velocity $v_{\rm F}$, being the characteristic velocity of conduction electrons in the metal. In the high (optical) frequency limit $\beta^2 = 3v_{\rm F}^2/5$ [26], [55]. Finally, $\epsilon_{\rm b}(\omega)$ is the background permittivity that includes all more complicated contributions such as interband transitions, and is obtained by fitting to experimental data [54], [56].

With these bulk response functions at hand, an analytical expression for the d-parameters can be found in the SRM by using Eq. (2a) [57]:

$$d_{\perp}^{\text{SRM}} = i \frac{\epsilon_{\text{m}} \epsilon_{\text{d}}}{\epsilon_{\text{m}} - \epsilon_{\text{d}}} \frac{\beta}{\omega_{\text{p}} \sqrt{\epsilon_{\text{b}}}} \left(\frac{\epsilon_{\text{b}}}{\epsilon_{\text{m}}} - 1\right)^{3/2}.$$
 (4)

The magnitude and behavior of the SRFs are investigated by computing $d_{\perp}^{\rm SRM}$ analytically for gold interfacing

different dielectric materials in Figure 1(b). For all frequencies under consideration here, $Re\{d_{\perp}^{SRM}\}$ < 0, indicating electron spill-in for the conduction electrons in gold, whose work function is relatively high. Such spill-in has previously been associated with core electron screening in noble metals [58], and is at odds with what is typically seen in jellium metals with lower work functions (e.g., Na), which exhibit spill-out and therefore a positive perpendicular Feibelman parameter [42]. Figure 1(b) also reveals that the magnitude of d_{\perp}^{SRM} becomes larger for dielectric media with higher permittivity, resulting in a pronounced increase of the spill-in at lower frequencies. For instance $d_{\perp}^{\rm SRM}$ approaches $d_{\perp}^{\rm SRM} pprox$ -0.35 Å at lower frequencies when the dielectric permittivity is $\epsilon_{\rm d}=$ 1, but goes towards $d_{\perp}^{\rm SRM}\approx-$ 2.8 Å for $\epsilon_{\rm d}=$ 8. The d_{\perp}^{SRM} obtained using Eq. (4) are in excellent quantitative agreement with atomistic simulations of metal films [46], while also capturing the same degree of spill-in inferred from recent experiments [36].

2.2 Semi-infinite metal films

The influence of the SRFs can manifest as a change in the emission properties of a QE positioned near a metal film at $\mathbf{r}=(x,y,h)$, i.e., a distance h from a metallic film extended in the xy plane, as illustrated schematically in Figure 1(a). Invoking the macroscopic quantum electrodynamics formalism detailed in the SI [59]–[63] for a QE characterized as a two-level system with transition energy $\hbar\varepsilon$ and dipole moment \mathbf{p} , the total QE spontaneous emission rate is

$$\Gamma = \Gamma_0 + \frac{2\mu_0}{\hbar} \varepsilon^2 \text{Im} \{ \mathbf{p}^* \cdot \mathcal{G}_{\varepsilon}^{\text{ref}}(\mathbf{r}, \mathbf{r}) \cdot \mathbf{p} \}, \tag{5}$$

where $\Gamma_0=\varepsilon^3|\mathbf{p}|^2/3\pi\varepsilon_0\hbar c^3$ is the vacuum decay rate, while the shift in the bare emitter transition frequency due to the photonic environment – the Lamb shift – is

$$\delta \varepsilon = \frac{\mu_0}{\pi \hbar} \mathcal{P} \int_0^\infty d\omega \frac{\omega^2}{\varepsilon - \omega} \operatorname{Im} \{ \mathbf{p}^* \cdot \mathcal{G}_{\omega}^{\text{ref}}(\mathbf{r}, \mathbf{r}) \cdot \mathbf{p} \}, \quad (6)$$

with \mathcal{P} denoting the principal value of the integral. The above expressions depend on the reflected part of the Green's tensor $\mathcal{G}^{\mathrm{ref}}_{\omega}$ at the QE location, which quantifies the QE self-interaction mediated by the metal–dielectric interface [64]. For a dipole oriented perpendicular to the metal surface, i.e., $\mathbf{p} = p\hat{\mathbf{z}}$, the nonvanishing Green's tensor component entering Eqs. (5) and (6) reads as

$$\mathcal{G}_{\omega,\perp}^{\text{ref}} = \frac{\mathrm{i}}{4\pi k_{\mathrm{d}}^2} \int_0^\infty \mathrm{d}k_{\parallel} k_{\parallel}^3 \frac{\mathrm{e}^{\mathrm{i}2k_{\mathrm{d},z}}}{k_{\mathrm{d},z}} r_{\mathrm{p}}(k_{\parallel},\omega),\tag{7}$$

where the Fresnel reflection coefficient for p-polarized light,

$$r_{\rm p} = \frac{\epsilon_{\rm m} k_{\rm d,z} - \epsilon_{\rm d} k_{\rm m,z} + (\epsilon_{\rm m} - \epsilon_{\rm d}) \left(i k_{\parallel}^2 d_{\perp} - i k_{\rm d,z} k_{\rm m,z} d_{\parallel} \right)}{\epsilon_{\rm m} k_{\rm d,z} + \epsilon_{\rm d} k_{\rm m,z} - (\epsilon_{\rm m} - \epsilon_{\rm d}) \left(i k_{\parallel}^2 d_{\perp} + i k_{\rm d,z} k_{\rm m,z} d_{\parallel} \right)},$$
(8)

depends on the optical wavevector \mathbf{k}_j in a medium of permittivity ϵ_j for $j \in \{d,m\}$, with normal component $k_{j,z} = \sqrt{\epsilon_j \omega^2/c^2 - {k_\parallel}^2 + \mathrm{i}0^+}$ and conserved parallel component k_\parallel , as well as on the SRFs that modify the electromagnetic boundary conditions at the metal–dielectric interface.

Using the above expressions, we compute the enhancement in spontaneous emission - quantified by the Purcell factor Γ/Γ_0 – along with the Lamb shift $\delta \varepsilon$ for a QE in a medium with permittivity ϵ_1 that is placed a distance h from a gold interface. In Figure 1(c) and (d), the Purcell factor and Lamb shift are respectively presented in calculations adopting a fixed vacuum permittivity $\epsilon_1 = 1$ at separations h indicated in the legend of Figure 1(c) when omitting (dashed curves) and including (solid curves) SRFs. In the cases considered here, the SRFs are found to introduce damping and spectral shifts in prominent plasmonic features of the Purcell factor and Lamb shift that become increasingly important as the QE is brought extremely close to the metal-dielectric interface. However, the considered OE separation distances $h \ge 2$ nm ensure that the local Feibelman formalism remains valid, while even smaller distances would motivate the use of either ab-initio computations or the introduction of wave-vector-dependent d-parameters [40], [44]. As shown in the SI, this conclusion is supported by the excellent agreement exhibited by the Purcell factors predicted using SRFs and their counterparts computed directly from the SRM by adopting a longitudinal dielectric function within the HDM, i.e., invoking the same level of theory used to obtain analytical d_{\perp}^{SRM} in Eq. (4), while the Feibelman SRF formalism advantageously admits closed-form expressions for the Green's tensor in the quasistatic regime. The effect of the surface response in quantum electrodynamical phenomena is further amplified when the permittivity of the dielectric medium is increased to enhance spill-in of the interfacing metal electron gas, as revealed in Figure 1(d) and (e) by the change in Purcell factor and Lamb shift, respectively, for a QE with fixed separation h = 2 nm and varying environment-permittivity ϵ_1 . The above results underscore the importance of nonclassical surface effects in quantum electrodynamics at a metal-dielectric interface, particularly for dielectric media with high permittivity.

2.3 Surface response of thin films

Thin metal films present larger surface-to-volume ratios that should enhance SRF contributions in nanoscale

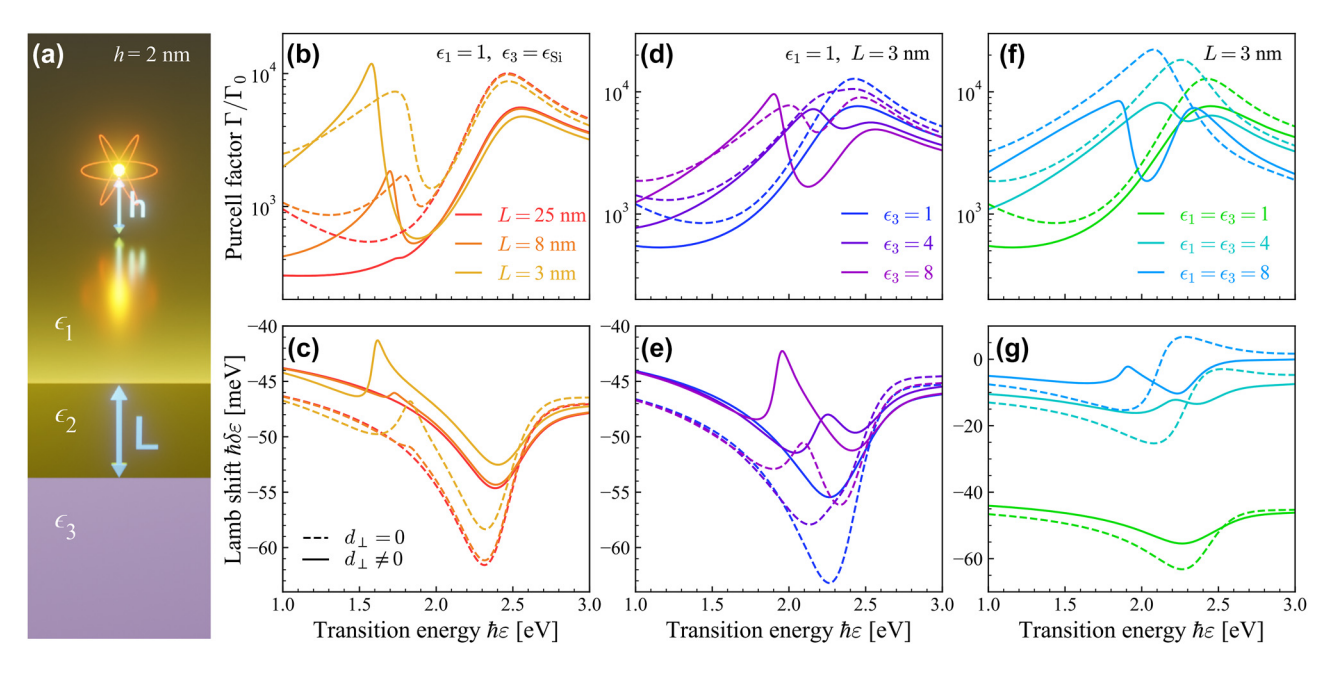


Figure 2: Enhanced surface effects in the quantum electrodynamic response of thin metal films. (a) Schematic of a QE at distance h from a thin metal film of width L. In panels (b-q) the calculated Purcell factors and Lamb shifts experienced by a QE with transition dipole moment d=1 e nm placed a distance h = 2 nm above a film are shown for cases with (solid curves) and without (dashed curves) incorporating SRFs in the optical response. Panels (b, c) show results for a QE in vacuum ($\epsilon_1 = 1$) close to an Au film of varying thickness, on a Si substrate with permittivity ϵ_3 interpolated from experimental data [65]. For a film with L=3 nm, panels (d, e) show the effect of substrate permittivity ϵ_3 when the QE is in vacuum, while panels (f, g) show the quantum electrodynamic response when the Au film is embedded in a medium with varying permittivity $\epsilon_1 = \epsilon_2$.

light-matter interactions, while also exhibiting higher sensitivity to screening from interfacing dielectric media. In Figure 2 we explore the interaction of a QE in a dielectric medium ϵ_1 placed a distance h above a thin gold film with permittivity ϵ_2 and thickness L on a substrate with permittivity ϵ_3 , as illustrated schematically in Figure 2(a). The film reflection coefficients are

$$R_{\alpha} = r_{\alpha}^{(12)} + \frac{t_{\alpha}^{(21)} t_{\alpha}^{(12)} r_{\alpha}^{(23)} e^{i2k_{2,z}L}}{1 - r_{\alpha}^{(21)} r_{\alpha}^{(23)} e^{i2k_{2,z}L}}$$
(9)

for $\alpha \in \{s, p\}$ polarization, where $r_{\alpha}^{(jj')}$ and $t_{\alpha}^{(jj')}$ are reflection and transmission coefficients, respectively, associated with light impinging from a medium with permittivity ϵ_i on an interface with permittivity $\epsilon_{i'}$, which contain the dependence on SRFs as detailed in the SI.

We explore the influence of SRFs on the Purcell factor and Lamb shift in Figure 2(b) and (c), respectively, for a QE in vacuum ($\epsilon_1 = 1$) above gold films ($\epsilon_2 = \epsilon_{Au}$) with varying thickness L deposited on silicon ($\epsilon_3 = \epsilon_{Si}$, obtained from interpolated experimental data in Ref. [65]) by replacing the single-interface reflection coefficient in Eq. (7) with that of Eq. (9) obtained with (solid curves) and without (dashed curves) SRFs. Note that the smallest film thickness considered is L=3 nm, well above the magnitude of dparameters in Figure 1(b) associated with electron spill-in.

In thin metal films, the largest deviation from a classical description of the photonic environment is predicted for the thinnest film, where a second plasmonic peak is present at low energies coming from the plasmonic mode at the lower Si-Au interface. Interestingly, low-energy features in the Purcell factor and Lamb shift are enhanced by SRFs in the thinnest film, presumably due to the large negative real values of d_{\perp} that describe spill-in of the metal film charge density that effectively reduces the thickness of the free electron gas and boosts plasmonic field confinement. In contrast, high-energy features in the emission spectra experience greater surface damping quantified by the imaginary part of d_{\perp} . Similar behavior is seen by considering substrates with different dielectric permittivities, as shown in Figure 2(d) and (e), where an additional peak emerges when substrates with high permittivities are considered. In Figure 2(f) and (g) we consider the impact of SRFs on the QE self-interaction when $\epsilon_1 = \epsilon_2$ and the metal film is embedded in a high-permittivity dielectric, where plasmon hybridization between the two surfaces may yield a low-energy bonding mode and a higher energy antibonding mode [66], [67]. For $\epsilon_1 = \epsilon_3 = 8$ in Figure 2(f) one can see the splitting associated with the hybridization between the two surfaces when including d-parameters but not when classically computing the Purcell factor. This can be interpreted as the SRFs effectively decreasing the width of the thin film and hence increasing plasmon hybridization through electron spill-in (a negative d_{\perp}), a phenomenon that is enhanced when high-permittivity media interface the gold film.

2.4 Spherical metallic nanoparticles

Metallic NPs supporting localized plasmon resonances are quintessential light-focusing elements in nanophotonics that are conveniently described using Mie theory. As depicted in Figure 3(a), we consider the light emission

properties of an emitter characterized by a radially-oriented dipole moment in a medium with permittivity ϵ_1 at a distance r from the center of a spherical metallic NP with radius a and permittivity ϵ_2 . The quantum electrodynamic response is quantified by the reflected part of the Green's function

$$G_{\varepsilon}^{\text{ref}}(r) = -\frac{\mathrm{i}k_1}{4\pi} \sum_{l} l(l+1)(2l+1)a_l \left[\frac{h_l^{(1)}(k_1 r)}{k_1 r} \right]^2, \tag{10}$$

where

$$a_{l} = \frac{\epsilon_{2} \Psi_{l}'(x_{1}) j_{l}(x_{2}) - \epsilon_{1} j_{l}(x_{1}) \Psi_{l}'(x_{2}) + (\epsilon_{2} - \epsilon_{1}) \left[\bar{d}_{\perp} j_{l}(x_{1}) j_{l}(x_{2}) + \bar{d}_{\parallel} \Psi_{l}'(x_{1}) \Psi_{l}'(x_{2}) \right]}{\epsilon_{2} j_{l}(x_{2}) \xi_{l}'(x_{1}) - \epsilon_{1} h_{l}^{(1)}(x_{1}) \Psi_{l}'(x_{2}) + (\epsilon_{2} - \epsilon_{1}) \left[\bar{d}_{\perp} h_{l}^{(1)}(x_{1}) j_{l}(x_{2}) + \bar{d}_{\parallel} \Psi_{l}'(x_{2}) \xi_{l}'(x_{1}) \right]}$$

$$(11)$$

are Mie coefficients that are linearized in the Feibelman d-parameters, as reported in Ref. [42], normalized according to $\bar{d}_{\perp} \equiv l(l+1)d_{\perp}/a$ and $\bar{d}_{\parallel} \equiv d_{\parallel}/a$, while j_l and $h_l^{(1)}$ are spherical Bessel and Hankel-of-the-first-kind functions, respectively, of the normalized parameter $x_j \equiv k_j a$ that also enters the derivatives of the Riccati-Bessel functions $\Psi_l'(x) = \partial_x \left[x j_l(x) \right]$ and $\xi_l'(x) = \partial_x \left[x h_l^{(1)}(x) \right]$.

With the above expressions at hand, the Purcell enhancement and Lamb shift of a QE near a spherical Au NP are found for a series of radii in Figure 3(b) and (c). The d-parameters in Eq. (11) go as $l(l+1)d_{\perp}/a$ and d_{\parallel}/a , meaning that their relative contribution increases for smaller NP radius and higher multipolar modes. As the higher multipolar modes influence the Green's function for smaller distances between the QE and the NP, as seen in Eq. (10), one would expect the influence of SRFs to increase for smaller radii, in agreement with the results in Figure 3(b) and (c). In addition, when varying the background permittivity rather than the radius of the NP, as in Figure 3(d) and (f), one sees that the larger permittivity ensures a larger deviation from the classical results when including the SRF, an effect which is particularly noticeable in the Lamb shift. Incidentally, as we show in the SI, the above results obtained using Mie theory are qualitatively reproduced by incorporating SRFs in the multipolar polarizability obtained in the quasistatic approximation, which is well-justified when the size of the NP and the QE-NP separation are small. Remarkably, the Feibelman SRFs describing planar metal-dielectric interfaces can be used in Mie theory to accurately reproduce the Purcell factors obtained by numerically integrating over optical wave vectors in nonlocal electrodynamic

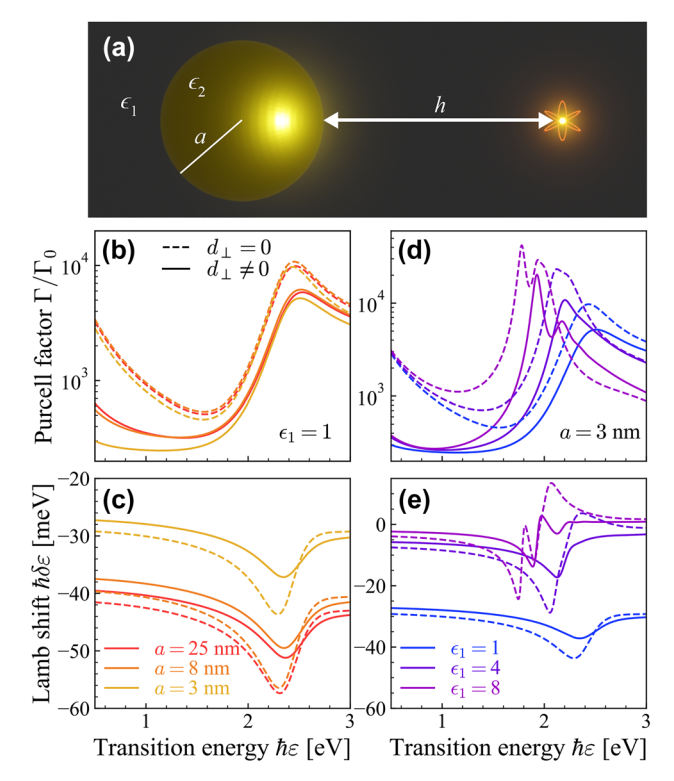


Figure 3: Surface effects in quantum light emission near a spherical plasmonic nanoparticle. (a) Schematic of a QE located in a medium with permittivity ϵ_1 at a distance h from the surface of a spherical NP with permittivity ϵ_2 and radius a. Panels (b, c) show the Purcell factor and Lamb shift of a QE in vacuum ($\epsilon_1=1$) close to Au NPs with radii indicated in (c), while panels (d, e) show results obtained for a small NP with fixed radius a=3 nm and varying background dielectric constant. Results are obtained for a QE transition dipole moment d=1 e nm oriented normally to and placed h=2 nm from the outer surface of the NP, with solid and dashed curves indicating results obtained with and without including SRFs, respectively.

models of spherical NPs following the combined SRM and HDM approach of Refs. [51], [52], although the analytical *d*-parameter model underestimates nonlocal damping in cases of extreme NP curvature (see SI).

2.5 Surface response effects in spherical core-shell nanoparticles

Compared to spherical NPs, the additional metal-dielectric interface in spherical dielectric core-metal shell NPs (CSNPs) leads to a more involved dependence on surface effects in the optical response, as indicated by the lengthy analytical expressions reported in the SI for both the associated Mie coefficients and the quasistatic multipolar polarizability. For a dipole oriented in the radial direction and placed a distance h from the center of a CSNP with core radius a and shell radius b, as illustrated in Figure 4(a), the Purcell factor and Lamb shift corresponding to the solutions from Mie theory are plotted in Figure 4(b)-(g). The sharper spectral features in the classical estimation of the Purcell factor and Lamb shift are slightly damped and blueshifted by SRFs, which can also produce qualitative changes around these multipolar modes. Here, the dparameters appear in the polarizability as $l(l+1)d_{\perp}/R$ for $R \in \{a, b\}$, with the higher-order modes tending to exhibit larger SRF-contributions resulting in larger blueshifting and damping. Similarly to the spherical NP, the influence of SRFs is most prominent in higher-order multipolar modes, with

the *d*-parameters corresponding to the different interfaces contributing more when the radius of the corresponding interface is small. This can be seen in Figure 4(b) and (c), where the introduction of *d*-parameters to the CSNP with the thinnest shell generally damps and influences the Purcell factor and Lamb shift more as compared to CSNPs with thicker shells. We remark that qualitatively similar results are obtained by introducing SRFs in a quasistatic description of the CSNP response, which conveniently leads to analytical expressions for the multipolar polarizability (see SI).

In Figure 4(d)–(g) we explore the impact of SRFs in the quantum electrodynamic response of the CSNP when either the core permittivity or the surrounding permittivity are varied. In the former case, oscillations in the QE Purcell factor and Lamb shift associated with the core–shell interface are significantly blueshifted and damped in the higher-frequency regime when introducing the SRF for high-permittivity cores. In the latter situation, choosing silicon dioxide (SiO₂)–also known as silica–as the core while the surrounding permittivity is varied, the high-frequency peak associated with the shell-surrounding interface exhibits similar but more pronounced damping and spectral shifting when including SRFs.

The spontaneous emission spectrum of a QE positioned in a photonic environment can be written in terms of the Green's function characterizing the environment as

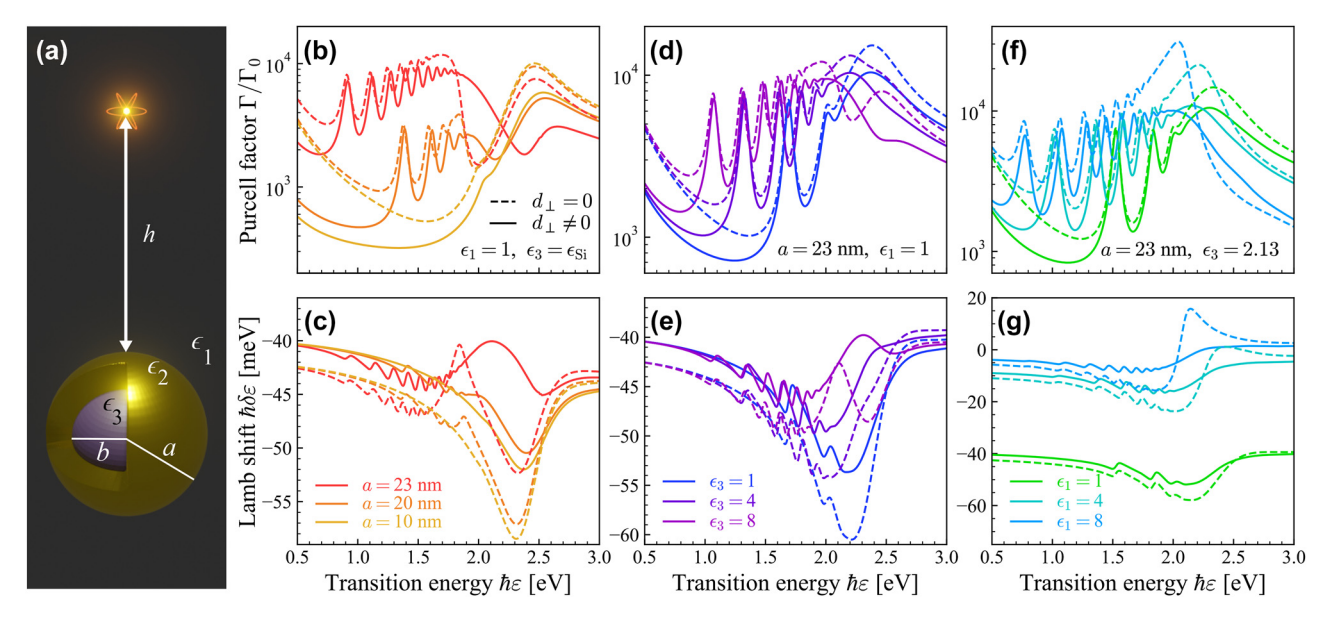


Figure 4: Dependence of the Lamb shift and Purcell factor on surface effects in a plasmonic CSNP. (a) Schematic of a QE at distance h from the surface of a CSNP with core radius a and shell radius b. (b, c) Show, respectively, the Purcell enhancement and Lamb shift of a QE close to a CSNP with a Si core (ϵ_3 from Ref. [65]) and Au shell (b=25 nm) at varying core-radii as indicated in (c). (d, e) Consider a core with fixed radius of a=23 nm and varying permittivity. Lastly, in panels (f, g) the core is fixed with $\epsilon_3=2.13$ to mimic SiO₂ and the environment permittivity ϵ_1 is varied. Results are obtained for a QE with transition dipole moment d=1 e nm placed normally to and a distance h=2 nm from the outer NP surface, taking the environment permittivity $\epsilon_1=1$ except in (f, g).

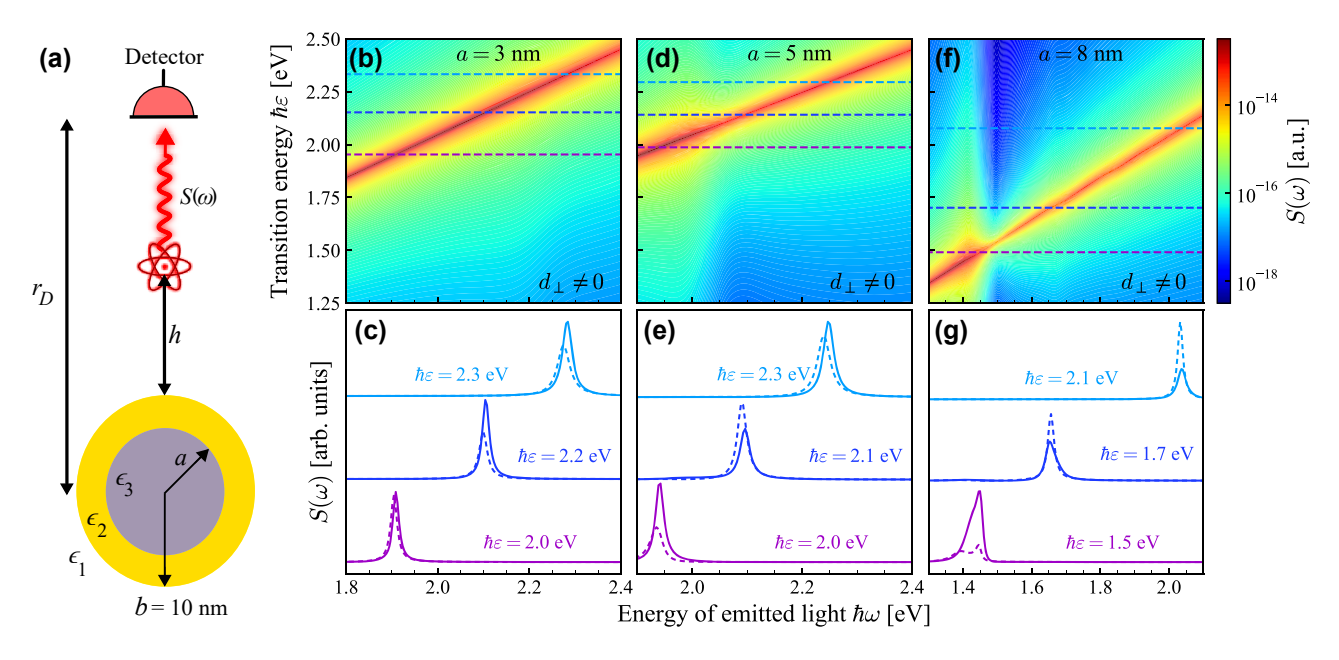


Figure 5: Detection of surface response effects in spontaneous emission produced near a plasmonic nanostructure. (a) Schematic illustration of a QE in a medium with permittivity ε_1 at distance h from the outer surface of a CSNP, with shell radius (permittivity) h (ε_2) and core radius (permittivity) h (θ_2) a

$$S(\omega) = \left| \frac{\mu_0 \omega^2 \mathbf{p}^* \cdot \mathcal{G}_{\omega}(\mathbf{r}_{\mathrm{D}}, \mathbf{r})(\omega + \varepsilon)}{\varepsilon^2 - \omega^2 - i\omega\gamma_{\mathrm{d}} - 2\mu_0 \varepsilon \omega^2 \mathbf{p}^* \cdot \mathcal{G}_{\omega}(\mathbf{r}, \mathbf{r}) \cdot \mathbf{p}/\hbar} \right|^2,$$
(12)

where ${\bf r}_{\rm D}$ denotes the detector position in the far field. The above expression is found in the weak excitation approximation by using the Wiener–Khinchin theorem and accounting for non-Markovian effects [64], [68], [69]. These spectra allow for the investigation of possible strong coupling regimes accessible in plasmon-emitter interactions, and of the impact of SRFs on experimental observables in these regimes.

The spectrum of the QE computed from Eq. (12) is displayed in Figure 5 for a CSNP with an Au shell of fixed outer radius b=10 nm and a Si core in Figure 5(b)–(g) with varying core radii as described in the figure caption. Because silicon is a dielectric material with a large permittivity in the frequency window of interest, any effects originating from SRFs should be more pronounced than those appearing in a CSNP with a lower permittivity core material such as SiO_2 . The d-parameters introduce a large visible blueshift in all cases considered in Figure 5, which is attributed to spill-in of the free electron distribution in the gold shell.

The spectra displayed in Figure 5 exhibit two peaks at some QE transition frequencies, which can be seen for $\hbar \varepsilon = 1.5$ eV in Figure 5(g). These peaks are significantly influenced by the SRFs; the amplitude of the spectrum is here enhanced by the SRFs and the two classical peaks coalesce into one peak. It is clear from Figure 5 that the inclusion of d-parameters influences the spectrum dramatically with a generally more pronounced effect for the thinnest shell in Figure 5(g). This supports the claim that SRFs are particularly important for thin films or shells, where the surface-to-volume ratio is larger, allowing the SRFs to play a vital role in the optical response.

3 Conclusions

Quantum mechanical and nonlocal phenomena at metal-dielectric interfaces become important in the description of light–matter interactions on $\lesssim 10$ nm length scales. These phenomena impact the quantum electrodynamic response of an emitter in close proximity to noble metal nanostructures, as revealed here by the large differences in the Lamb shift and Purcell factor that emerge when comparing the

classical response of metallic nanostructures to the nonlocal response described in the Feibelman d-parameter formalism. In particular, the d-parameters obtained from the SRM predict a sizeable increase in d_{\perp} when high-permittivity media interface the noble metal, which is especially important when regarding complicated nanophotonic systems with multiple interfaces and increased surface-to-volume ratios. This finding is showcased for metal films and CSNPs that exhibit pronounced differences in the Lamb shift and Purcell factor of a nearby QE when thinner films or shells are considered, such that electron spill-in enhances plasmon hybridization. The influence of d-parameters on the spontaneous emission spectrum of a QE close to a noble metal nanostructure has similarly been investigated, where a large difference in the spectrum can be seen in the case of Si-Au CSNPs. The QE spectrum may be observed in experiments, and constitutes a route for experimentally determining the d-parameters by comparing the experimental results with theoretical modelling, similar to the strategy proposed in Ref. [53] for determining *d*-parameters using electron-beam spectroscopy. The analytical results presented here facilitate straightforward evaluation of the spectrum, Purcell factor, and Lamb shift of QEs close to commonly explored metallic nanostructure morphologies in both quasistatic and retarded regimes.

Acknowledgments: We thank P. A. D. Gonçalves and C. Wolff for stimulating discussions. J.D.C. is a Sapere Aude research leader supported by Independent Research Fund Denmark (grant no. 0165-00051B). N.A.M. is a VILLUM Investigator supported by VILLUM FONDEN (Grant No. 16498). The Center for Polariton-driven Light-Matter Interactions (POLIMA) is funded by the Danish National Research Foundation (Project No. DNRF165).

Research funding: Independent Research Fund Denmark (grant no. 0165-00051B); VILLUM FONDEN (Grant No. 16498); Danish National Research Foundation (Project No. DNRF165).

Author contributions: All authors have accepted responsibility for the entire content of this manuscript and approved its submission.

Conflict of interest: Authors state no conflict of interest. Data availability: The datasets generated during and analyzed during the current study are available from the corresponding author on reasonable request.

References

[1] X. Zhang, Y. L. Chen, R.-S. Liu, and D. P. Tsai, "Plasmonic photocatalysis," Rep. Prog. Phys., vol. 76, no. 4, p. 046401, 2013.

- [2] A. Streltsov, G. Adesso, and M. B. Plenio, "Colloquium: quantum coherence as a resource," Rev. Mod. Phys., vol. 89, no. 4, p. 041003,
- [3] P. Dombi, et al., "Strong-field nano-optics," Rev. Mod. Phys., vol. 92, no. 2, p. 025003, 2020.
- [4] H. Mertens and A. Polman, "Plasmon-enhanced erbium luminescence," Appl. Phys. Lett., vol. 89, no. 21, p. 211107, 2006.
- [5] J. Yan, Z. Yuan, and S. Gao, "End and central plasmon resonances in linear atomic chains," Phys. Rev. Lett., vol. 98, no. 21, p. 216602, 2007.
- [6] M. Nečada, J.-P. Martikainen, and P. Törmä, "Quantum emitter dipole – dipole interactions in nanoplasmonic systems," Int. J. Mod. Phys. B, vol. 31, no. 24, p. 1740006, 2017.
- [7] J. D. Cox and F. J. García de Abajo, "Nonlinear atom-plasmon interactions enabled by nanostructured graphene," Phys. Rev. Lett., vol. 121, no. 25, p. 257403, 2018.
- [8] D. Chang, A. S. Sørensen, P. Hemmer, and M. D. Lukin, "Quantum optics with surface plasmons," Phys. Rev. Lett., vol. 97, no. 5, p. 053002, 2006.
- [9] S. I. Bozhevolnyi and N. A. Mortensen, "Plasmonics for emerging quantum technologies," Nanophotonics, vol. 6, no. 5, p. 1185, 2017.
- [10] S. I. Bozhevolnyi and J. B. Khurgin, "The case for quantum plasmonics," Nat. Photon., vol. 11, no. 7, p. 398, 2017.
- A. I. Fernández-Domínguez, S. I. Bozhevolnyi, and N. A. Mortensen, "Plasmon-enhanced generation of nonclassical light," ACS Photonics, vol. 5, no. 9, p. 3447, 2018.
- [12] J. L. O'Brien, A. Furusawa, and J. Vučković, "Photonic quantum technologies," Nat. Photon., vol. 3, no. 12, p. 687, 2009.
- [13] N. A. Mortensen, "Mesoscopic electrodynamics at metal surfaces: from quantum-corrected hydrodynamics to microscopic surface-response formalism," Nanophotonics, vol. 10, no. 10,
- [14] J. M. Pitarke, V. M. Silkin, E. V. Chulkov, and P. M. Echenique, "Theory of surface plasmons and surface-plasmon polaritons," Rep. Prog. Phys., vol. 70, no. 1, p. 1, 2006.
- [15] J. A. Scholl, A. L. Koh, and J. A. Dionne, "Quantum plasmon resonances of individual metallic nanoparticles," Nature, vol. 483, no. 7390, p. 421, 2012.
- [16] S. Raza, S. I. Bozhevolnyi, M. Wubs, and N. A. Mortensen, "Nonlocal optical response in metallic nanostructures," J. Phys. Condens. Matter, vol. 27, no. 18, p. 183204, 2015.
- [17] Á. Rodríguez Echarri, J. D. Cox, and F. J. García de Abajo, "Quantum effects in the acoustic plasmons of atomically thin heterostructures," Optica, vol. 6, no. 5, p. 630, 2019.
- [18] S. Raza, G. Toscano, A.-P. Jauho, M. Wubs, and N. A. Mortensen, "Unusual resonances in nanoplasmonic structures due to nonlocal response," Phys. Rev. B, vol. 84, no. 12, p. 121412, 2011.
- [19] N. A. Mortensen, S. Raza, M. Wubs, T. Søndergaard, and S. I. Bozhevolnyi, "A generalized non-local optical response theory for plasmonic nanostructures," Nat. Commun., vol. 5, no. 1, p. 3809,
- [20] G. Toscano, et al., "Resonance shifts and spill-out effects in self-consistent hydrodynamic nanoplasmonics," Nat. Commun., vol. 6, no. 1, p. 7132, 2015.
- [21] C. Ciracì and F. Della Sala, "Quantum hydrodynamic theory for plasmonics: impact of the electron density tail," Phys. Rev. B, vol. 93, no. 20, p. 205405, 2016.
- [22] A. Trügler, U. Hohenester, and F. J. García de Abajo, "Plasmonics simulations including nonlocal effects using a boundary element

- method approach," Int. J. Mod. Phys. B, vol. 31, no. 24, p. 1740007,
- [23] M. Kupresak, X. Zheng, G. A. E. Vandenbosch, and V. V. Moshchalkov, "Appropriate nonlocal hydrodynamic models for the characterization of deep-nanometer scale plasmonic scatterers," Adv. Theory Simul., vol. 3, no. 1, p. 1900172, 2020.
- [24] Y. Eremin, A. Doicu, and T. Wriedt, "Discrete sources method for modeling of the influence of the non-local effect on the absorption of bimetallic core-shell non-spherical plasmonic nanoparticles," J. Quant. Spectrosc. Radiat. Transf., vol. 277, p. 107994, 2021.
- [25] C. Mystilidis, X. Zheng, and G. A. E. Vandenbosch, "OpenSANS: a semi-analytical solver for nonlocal plasmonicS," Comput. Phys. Commun., vol. 284, p. 108609, 2023.
- [26] G. Wegner, D.-N. Huynh, N. A. Mortensen, F. Intravaia, and K. Busch, "Halevi's extension of the Euler-Drude model for plasmonic systems," Phys. Rev. B, vol. 107, no. 11, p. 115425, 2023.
- [27] J. Zuloaga, E. Prodan, and P. Nordlander, "Quantum description of the plasmon resonances of a nanoparticle dimer," Nano Lett., vol. 9, no. 2, p. 887, 2009.
- [28] T. V. Teperik, P. Nordlander, J. Aizpurua, and A. G. Borisov, "Robust subnanometric plasmon ruler by rescaling of the nonlocal optical response," Phys. Rev. Lett., vol. 110, no. 26, p. 263901, 2013.
- [29] A. Varas, P. García-González, J. Feist, F. García-Vidal, and A. Rubio, "Quantum plasmonics: from jellium models to ab initio calculations," Nanophotonics, vol. 5, no. 3, p. 409, 2016.
- [30] W. Zhu, et al., "Quantum mechanical effects in plasmonic structures with subnanometre gaps," Nat. Commun., vol. 7, no. 1, p. 11495, 2016.
- [31] W. Yan, "Hydrodynamic theory for quantum plasmonics: linear-response dynamics of the inhomogeneous electron gas," Phys. Rev. B, vol. 91, no. 11, p. 115416, 2015.
- [32] P. E. Stamatopoulou and C. Tserkezis, "Finite-size and quantum effects in plasmonics: manifestations and theoretical modelling," Opt. Mater. Express, vol. 12, no. 5, p. 1869, 2022.
- [33] P. J. Feibelman, "Surface electromagnetic fields," Prog. Surf. Sci., vol. 12, no. 4, p. 287, 1982.
- [34] W. Yan, M. Wubs, and N. A. Mortensen, "Projected dipole model for quantum plasmonics," Phys. Rev. Lett., vol. 115, no. 13, p. 137403,
- [35] T. Christensen, W. Yan, A.-P. Jauho, M. Soliačić, and N. A. Mortensen, "Quantum corrections in nanoplasmonics: shape, scale, and material," Phys. Rev. Lett., vol. 118, no. 15, p. 157402, 2017.
- [36] Y. Yang, et al., "A general theoretical and experimental framework for nanoscale electromagnetism," Nature, vol. 576, no. 7786, p. 248, 2019.
- [37] C. Tserkezis, "Towards quantum nanophotonics: from quantum-informed plasmonics to strong coupling," Dr. Techn. thesis, University of Southern Denmark, 2021.
- [38] V. Karanikolas, et al., "Quantum surface effects in strong coupling dynamics," Phys. Rev. B, vol. 104, no. 20, p. L201405, 2021.
- [39] M. K. Dezfouli, C. Tserkezis, N. A. Mortensen, and S. Hughes, " Nonlocal quasinormal modes for arbitrarily shaped three-dimensional plasmonic resonators," Optica, vol. 4, no. 12, p. 1503, 2017.
- [40] A. Babaze, et al., "Quantum surface effects in the electromagnetic coupling between a quantum emitter and a plasmonic nanoantenna: time-dependent density functional theory vs. semiclassical Feibelman approach," Opt. Express, vol. 30, no. 12, p. 21159, 2022.

- [41] N. A. Mortensen, et al., "Surface-response functions obtained from equilibrium electron-density profiles," Nanophotonics, vol. 10, no. 14, p. 3647, 2021.
- [42] P. A. D. Gonçalves, T. Christensen, N. Rivera, A.-P. Jauho, N. A. Mortensen, and M. Soljačić, "Plasmon – emitter interactions at the nanoscale," Nat. Commun., vol. 11, no. 1, p. 366, 2020.
- [43] P. A. D. Gonçalves, *Plasmonics and Light—Matter Interactions in* Two-Dimensional Materials and in Metal Nanostructures: Classical and Quantum Considerations, Cham, Springer Nature, 2020.
- [44] A. Babaze, T. Neuman, R. Esteban, J. Aizpurua, and A. G. Borisov, "Dispersive surface-response formalism to address nonlocality in extreme plasmonic field confinement," Nanophotonics, vol. 12, no. 16. p. 3277, 2023.
- [45] G. W. Ford and W. H. Weber, "Electromagnetic interactions of molecules with metal surfaces," Phys. Rep., vol. 113, no. 4, p. 195, 1984.
- [46] Á. Rodríguez Echarri, P. A. D. Gonçalves, C. Tserkezis, F. J. García de Abajo, N. A. Mortensen, and J. D. Cox, "Optical response of noble metal nanostructures: quantum surface effects in crystallographic facets," Optica, vol. 8, no. 5, p. 710, 2021.
- [47] M. O. Scully and S. M. Zubairy, Quantum Optics, Cambridge, Cambridge University Press, 1997.
- [48] L. Novotny and B. Hecht, *Principles of Nano-Optics*, Cambridge, Cambridge University Press, 2012.
- [49] U. Hohenester, Nano and Quantum Optics, Cham, Springer, 2020.
- [50] C.-H. Chang, N. Rivera, J. D. Joannopoulos, M. Soljačić, and I. Kaminer, "Constructing "designer atoms" via resonant graphene-induced Lamb shifts," ACS Photonics, vol. 4, no. 12, p. 3098, 2017.
- [51] F. J. García de Abajo, "Nonlocal effects in the plasmons of strongly interacting nanoparticles, dimers, and waveguides," J. Phys. Chem. C, vol. 112, no. 46, p. 17983, 2008.
- [52] C. David and F. J. García de Abajo, "Spatial nonlocality in the optical response of metal nanoparticles," J. Phys. Chem. C, vol. 115, no. 40, p. 19470, 2011.
- [53] P. A. D. Gonçalves and F. J. García de Abajo, "Interrogating quantum nonlocal effects in nanoplasmonics through electron-beam spectroscopy," Nano Lett., vol. 23, no. 10, p. 4242,
- [54] P. G. Etchegoin, E. C. Le Ru, and M. Meyer, "An analytic model for the optical properties of gold," J. Chem. Phys., vol. 125, no. 16, p. 164705, 2006.
- [55] P. Halevi, "Hydrodynamic model for the degenerate free-electron gas: generalization to arbitrary frequencies," Phys. Rev. B, vol. 51, no. 12, p. 7497, 1995.
- [56] P. B. Johnson and R.-W. Christy, "Optical constants of the noble metals," Phys. Rev. B, vol. 6, no. 12, p. 4370, 1972.
- [57] M. Svendsen, C. Wolff, A.-P. Jauho, N. A. Mortensen, and C. Tserkezis, "Role of diffusive surface scattering in nonlocal plasmonics," J. Phys. Condens. Matter, vol. 32, no. 39, p. 395702,
- [58] A. Liebsch, "Surface-plasmon dispersion and size dependence of Mie resonance: silver versus simple metals," Phys. Rev. B, vol. 48, no. 15, p. 11317, 1993.
- [59] E. Forati, G. W. Hanson, and S. Hughes, "Graphene as a tunable THz reservoir for shaping the Mollow triplet of an artificial atom via plasmonic effects," Phys. Rev. B, vol. 90, no. 8, p. 085414, 2014.
- [60] R.-C. Ge, C. Van Vlack, P. Yao, J. F. Young, and S. Hughes, "Accessing quantum nanoplasmonics in a hybrid quantum

- dot metal nanosystem: mollow triplet of a quantum dot near a metal nanoparticle," Phys. Rev. B, vol. 87, no. 20, p. 205425, 2013.
- [61] T. V. C. Antão and N. M. R. Peres, "Two-level systems coupled to graphene plasmons: a Lindblad equation approach," Int. J. Mod. Phys. B, vol. 35, no. 20, p. 2130007, 2021.
- [62] M. H. Eriksen, J. E. Olsen, C. Wolff, and J. D. Cox, "Optoelectronic control of atomic bistability with graphene," Phys. Rev. Lett., vol. 129, no. 25, p. 253602, 2022.
- [63] S. Scheel and S. Y. Buhmann, "Macroscopic quantum electrodynamics - concepts and applications," Acta Phys. Slovaca, vol. 58, no. 5, p. 675, 2008.
- [64] P. Yao, C. Van Vlack, A. Reza, M. Patterson, M. Dignam, and S. Hughes, "Ultrahigh Purcell factors and Lamb shifts in slow-light metamaterial waveguides," Phys. Rev. B, vol. 80, no. 19, p. 195106, 2009.
- [65] M. A. Green, "Self-consistent optical parameters of intrinsic silicon at 300 K including temperature coefficients," Sol. Energy Mater. Sol. Cells, vol. 92, no. 11, p. 1305, 2008.

- [66] S. I. Bozhevolnyi and T. Søndergaard, "General properties of slow-plasmon resonant nanostructures: nano-antennas and resonators," Opt. Express, vol. 15, no. 17, p. 10869, 2007.
- [67] S. Raza, T. Christensen, M. Wubs, S. I. Bozhevolnyi, and N. A. Mortensen, "Nonlocal response in thin-film waveguides: loss versus nonlocality and breaking of complementarity," Phys. Rev. B, vol. 88, no. 11, p. 115401, 2013.
- [68] P. Meystre and M. Sargent, Elements of Quantum Optics, Berlin, Springer Science & Business Media, 2007.
- [69] C. V. Vlack, P. T. Kristensen, and S. Hughes, "Spontaneous emission spectra and quantum light-matter interactions from a strongly coupled quantum dot metal-nanoparticle system," Phys. Rev. B, vol. 85, no. 7, p. 075303, 2012.

Supplementary Material: This article contains supplementary material (https://doi.org/10.1515/nanoph-2023-0575).